Journal of Solid State Chemistry 184 (2011) 3273–3279

Contents lists available at SciVerse ScienceDirect

Journal of Solid State Chemistry

journal homepage: www.elsevier.com/locate/jssc

# Enhancement of oxygen vacancies and solar photocatalytic activity of zinc oxide by incorporation of nonmetal

Ashokrao B. Patil [a], Kashinath R. Patil [b], Satish K. Pardeshi [a,*]

[a] Department of Chemistry, University of Pune, Ganeshkhind, Pune 411007, India
[b] Center for Materials Characterization, National Chemical Laboratory, Pune 411008, India

ARTICLE INFO

*Article history:*
Received 26 April 2011
Received in revised form
7 October 2011
Accepted 10 October 2011
Available online 17 October 2011

*Keywords:*
Nonmetal doping
Enhanced oxygen vacancies
Photocatalysis
Sunlight
Bisphenol A

ABSTRACT

B-doped ZnO and N-doped ZnO powders have been synthesized by mechanochemical method and characterized by TG–DTA, XRD, SEM–EDX, XPS, UV–visible and photoluminescence (PL) spectra. X-ray diffraction data suggests the hexagonal wurtzite structure for modified ZnO crystallites and the incorporation of nonmetal expands the lattice constants of ZnO. The room temperature PL spectra suggest more number of oxygen vacancies exist in nonmetal-doped ZnO than that of undoped zinc oxide. XPS analysis shows the substitution of some of the O atoms of ZnO by nonmetal atoms. Solar photocatalytic activity of B-doped ZnO, N-doped ZnO and undoped ZnO was compared by means of oxidative photocatalytic degradation (PCD) of Bisphenol A (BPA). B-doped ZnO showed better solar PCD efficiency as compare to N-doped ZnO and undoped ZnO. The PCD of BPA follows first order reaction kinetics. The detail mechanism of PCD of Bisphenol A was proposed with the identification of intermediates such as hydroquinone, benzene-1,2,4-triol and 4-(2-hydroxypropan-2-yl) phenol.



## 1. Introduction

Photocatalysis is a promising technique for environmental detoxification, due to its ability to destroy a wide range of pollutants at ambient conditions. The most effective functional materials used for these processes are semiconductor oxides like $TiO_2$ and ZnO [1,2]. $TiO_2$ is most commonly used as a photocatalyst under UV light [3]. The photocatalytic degradation of organic contaminants using solar light could be highly economical compared with the processes using artificial UV radiation, which requires substantial amount of electrical power. Zinc oxide is a better option for $TiO_2$ because of its higher response towards solar energy [4–6]. Zinc oxide is an II–IV compound semiconductor with a wide and direct band gap of 3.2 eV and a large excitation binding energy of 60 meV [7]. The biggest advantage of ZnO is that it absorbs over a larger fraction of the solar spectrum and greater quantum efficiency than $TiO_2$ [8]. ZnO adopts the hexagonal wurtzite crystal structure, which has the space group $P6_3mc$ (No. 186). The atomic arrangements on low index planes of the hexagonal prism on ZnO are stoichiometric, with equal numbers of exposed $Zn^{2+}$ or $O^{2-}$ ions, while the basal planes and the pyramidal planes are strongly polar, consisting of sheets of $Zn^{2+}$ or $O^{2-}$. The polar planes of ZnO are playing very important role in solar photocatalytic reactions, because they favor the formation of more oxygen vacancies [9]. Many researchers have attempted to modify the electronic properties of zinc oxide in order to expand its optical absorption edge in to visible light region and to improve the photocatalytic activity [10–12]. These studies have demonstrated that doping with a nonmetal can provide an effective modification of electronic structure of ZnO. An appropriate amount of dopants can reduce the recombination of $e^-/h^+$ pairs and raise the photocatalytic activity.

Among the various methods, mechanochemical doping is one of the convenient methods employed for the incorporation of nonmetal elements into metal oxides [10,13]. Recently, we reported the synthesis of S-doped ZnO by mechanochemical grinding of zinc acetate, oxalic acid and thiourea, followed by calcination at 600 °C [14]. In present work, we report a simple mechanochemical route to synthesize B-doped ZnO and N-doped ZnO and the effect of nonmetal doping on solar photocatalytic activity for degradation of Bisphenol A.

## 2. Experimental

### 2.1. Materials

Zinc acetate (assay ≥98%), oxalic acid (assay 99.5%), boric acid (assay 99.5%), urea (assay 99.5%), Bisphenol A (assay 99%) and other required chemicals are of analytical grade, obtained from Merck Limited, Mumbai, India and were used without further purification. The 100 ppm Bisphenol A solution (BPA100) was prepared by using double distilled water.

* Corresponding author. Fax: +91 020 25691728.
*E-mail address:* skpar@chem.unipune.ac.in (S.K. Pardeshi).

0022-4596/$ - see front matter © 2011 Elsevier Inc. All rights reserved.
doi:10.1016/j.jssc.2011.10.016

### 2.2. Synthesis of nonmetal-doped zinc oxide

In a typical synthesis, 2.195 g of zinc acetate dihydrate and 1.512 g of oxalic acid were taken in agate mortar and mixture was ground for 10 min to obtain a paste of zinc oxalate dihydrate (ZO) and acetic acid. The existence of acetic acid was detected by its typical smell. The loss of acetic acid by-product in the form of fumes becomes a driving force for the reaction. The 0.1 g of urea was added to the above paste as a source of N and grinding process was continued for next 10 min to obtain zinc oxalate-urea (ZOU) precursor. The same procedure was repeated with 0.1 g of boric acid as a source of B to obtain zinc oxalate-boric acid (ZOB) precursor. The N-doped zinc oxide (NZnO) and B-doped zinc oxide (BZnO) crystallites were obtained by calcination of ZOU and ZOB powders, respectively, at 600 °C in air. The undoped zinc oxide (ZnO) was also synthesized by calcination of ZO at 600 °C for comparison.

### 2.3. Equipments and light source

Thermal decomposition of ZO, ZOU and ZOB were studied with thermogravimetry (Shimadzu TG-DTG-60 H). While, NZnO and BZnO crystallite were characterized by X-ray diffractometer (D-8 Advance Brukr AXS), UV–visible Spectrophotometer (UV-1601, Shimadzu), X-ray Photoelectron Spectra (XPS) and Photoluminescence (PL) spectra (Shimadzu, RF-5301PC). XPS were recorded with a V.G. Microtech (UK) unit ESCA 3000 spectrometer equipped with Mg $K\alpha$ X-ray source ($h\upsilon = 1253.6$ eV) and a hemispherical electron analyzer. The X-ray source was operated at 150 W. The residual pressure in the ion-pumped analysis chamber was maintained below $1.0 \times 10^{-9}$ Torr during data acquisition. The C1*s* peak at a binding energy 284.6 eV was taken as an internal standard. The accuracy of BE values was within $\pm 0.2$ eV. The photocatalytic reactions were carried out at ambient temperature under the irradiation of sunlight in batch photoreactor. The details of set up of photoreactor were already explained elsewhere [2]. The initial pH of suspension was recorded with the help of pH meter (EUTECH-pH510). The extent of photocatalytic degradation (PCD) of BPA at an interval of 30 min sunlight irradiation was primarily checked by means of decrease in absorbance at 276 nm ($\lambda_{max}$ of BPA). Complete mineralization of BPA was confirmed by chemical oxygen demand (COD) reduction method. The COD determination tests were performed according to standard dichromate method [15] using COD digester (SPECTRALAB 2015 M). The PCD efficiency was calculated using the following expression:

$$\eta = (\mathrm{COD_i} - \mathrm{COD_t}/\mathrm{COD_i}) \times 100 \quad (1)$$

where $\eta$ is the photocatalytic degradation efficiency, $\mathrm{COD_i}$ is the initial chemical oxygen demand and $\mathrm{COD_t}$ is the chemical oxygen demand at time *t*. The intensity of sunlight was checked by ferrioxalate actinometry [16]. The average photon flux calculated for sunlight was found to be $1.7 \times 10^{-7}$ Einstein $s^{-1}$ $cm^{-2}$. The PCD intermediates were identified by HPLC and GC–MS analysis. HPLC analysis was performed with a Shimadzu 20A instrument equipped with C18 column. The reusability of the photocatalyst was evaluated by reclaiming the photocatalyst after PCD reaction in the batch mode, washing, drying in electric oven at 110 °C and using it for BPA degradation under identical experimental conditions.

### 2.4. Photocatalytic degradation experiments

Solar photocatalytic activity of NZnO, BZnO and ZnO were compared by means of degradation of BPA. All the PCD experiments were carried out in duplicate and at an ambient temperature, without external supply of oxygen. The detailed procedure of PCD experiments is explained elsewhere [14]. The effect of fluctuation of sunlight intensity was eliminated by simultaneous run of PCD experiments.

## 3. Results and discussion

### 3.1. TG–DTA study

The thermal behavior of ZO, ZOU and ZOB is presented in Fig. 1. The main objective of TG–DTA study was to find out minimum possible calcination temperature at which ZO, ZOU and ZOB are converted to respective oxides. Thus the thermal weight loss of ZO occurs in two steps and above 406 °C the weight remains constant. Similarly, for ZOU and ZOB, above 419 °C and 430 °C, respectively, there was no weight loss. Hence, during the synthesis of nonmetal doped ZnO, ZOU and ZOB was calcined at 600 °C and respective oxides were characterized as N-doped ZnO and B-doped ZnO.

### 3.2. Characterization of BZnO and NZnO

#### 3.2.1. XRD pattern

Fig. 2 illustrates the XRD pattern of NZnO, BZnO and ZnO crystallite. The XRD data of all the powders exactly matches to that of JCPDS card No. 36-1451 for hexagonal wurtzite structure of ZnO. This suggests that the introduction of nitrogen or boron atoms does not change the ZnO crystal structure. The XRD pattern of BZnO and NZnO was found to be broader and slightly shifted towards a lower angle (0.3°) than that of pure ZnO (see inset of Fig. 2). This was due to fact that the replacement of O by B or N results in the shrinkage of some crystallite planes of ZnO structure which results into disordering of the crystallites of ZnO. This results into a compressive strain out of plane in BZnO and NZnO, possibly indicating the effective nonmetal incorporation in the lattice of nonmetal-doped ZnO. Similar observation was reported by Park et al. [17]. The crystallite size obtained by Scherer's formula from the 1 0 1 peak of the XRD pattern of ZnO, NZnO and BZnO was found to be 49, 43, and 35 nm, respectively.

#### 3.2.2. XPS analysis

The composition of nonmetal doped ZnO was determined by XPS analysis. Whole scanning XPS of BZnO have been shown in Fig. 3a. The fine XPS of $O_{1s}$ have been depicted in Fig. 3b, the peak

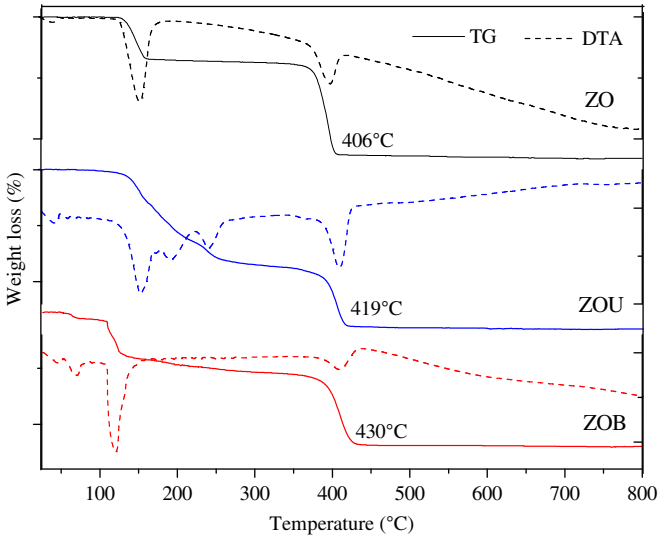


**Fig. 1.** TG–DTA curves: zinc oxalate (ZO), zinc oxalate urea (ZOU) precursor and zinc oxalate boric acid (ZOB) precursor.

at 530.10 eV was attributed to $O^{2-}$ ions of ZnO, while another at 531.73 eV is usually associated with the lower valant oxygen or adsorbed $O_2$ [18]. Fig. 3c shows the high resolution XPS for Zn 2*p* region of BZnO. The XPS peaks observed at 1021.5 and 1044.2 eV are assigned to Zn $2p_{3/2}$ and Zn $2p_{1/2}$ electrons, respectively, indicating Zn is in the $Zn^{2+}$ state. The high resolution XPS of B2*p* region (Fig. 3d) shows the peak positioned at 192 eV assigned to the B $2p_{1/2}$ electronic state of BZnO. Fig. 4a–d shows XPS of N-doped ZnO. The fine XPS of $O_{1s}$region of NZnO (Fig. 4b) shows peaks at 530.32 eV was attributed to $O^{2-}$ ions of ZnO, while that of 531.72 eV is attributed to lower valant oxygen or adsorbed $O_2$. Fig. 3c shows the high resolution XPS for Zn 2*p* region of NZnO. The XPS peaks observed at 1021.7 and 1044.5 eV are assigned to Zn $2p_{3/2}$ and Zn $2p_{1/2}$ electrons, respectively, indicating Zn is in the $Zn^{2+}$ state. The fine XPS of $N_{1s}$ region of NZnO displays peak centered at 397.6 eV was assigned to N atom in the form of Zn-N, indicating that some of the O atoms of ZnO are substituted by N. There is no any XPS peak at 401 and 402 eV in N 1*s* region of NZnO, which indicates that the Zn–O–N state is absent.

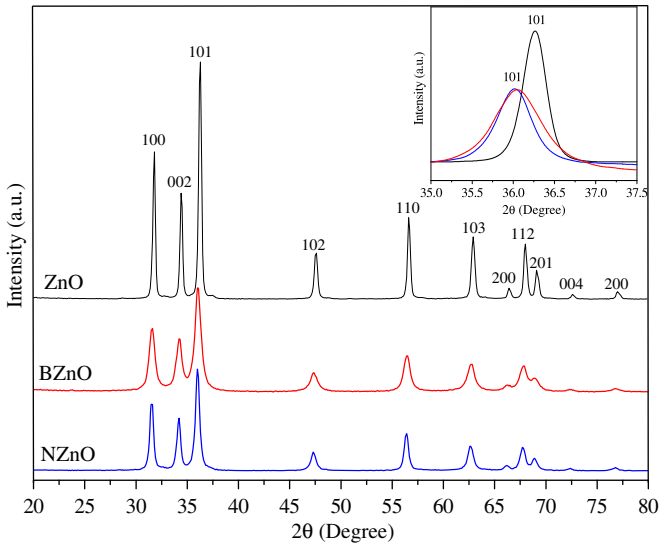


**Fig. 2.** XRD pattern of pure ZnO, B-doped ZnO and N-doped ZnO; inset: lower Bragg angle shift.

### 3.2.3. SEM–EDX analysis

The surface morphology and composition of nonmetal doped ZnO were analyzed using SEM–EDX studies. The SEM images of these samples (Fig. 5) show the single homogeneous phase with a porous sponge like morphology. Energy dispersive X-ray spectra (EDX) of N-doped and B-doped ZnO is shown in Fig. 6. EDX spectrum of N-doped ZnO shows peaks corresponding to Zn, O, and N while that of B-doped ZnO displays peak for B in addition to Zn and O. Quantitative analysis of EDX indicates that N-doped ZnO contains 2.8 wt% of N and B-doped ZnO contains 1.5 wt% of B. Both the samples of nonmetal doped ZnO are free from other impurities.

### 3.2.4. UV–visible and photoluminescence study

Typical UV–visible spectra of pure and modified ZnO are shown in Fig. 7. It is observed that when ZnO is doped with nonmetal (B or N); in addition to fall in absorption intensity the absorption wavelength of zinc oxide shifts towards longer wavelength. The $\lambda_{max}$ of undoped, N-doped and B-doped ZnO was found to be 375.7, 379 and 379.9 nm, respectively. Hence the band gap of pure ZnO (3.30 eV) becomes narrower for NZnO (3.27 eV) and BZnO (3.24 eV). The narrowing of band gap is useful for solar light mediated photocatalysis as it helps to absorb light of longer wavelength. The PL spectra of NZnO, BZnO and ZnO with the excitation wavelength of 300 nm

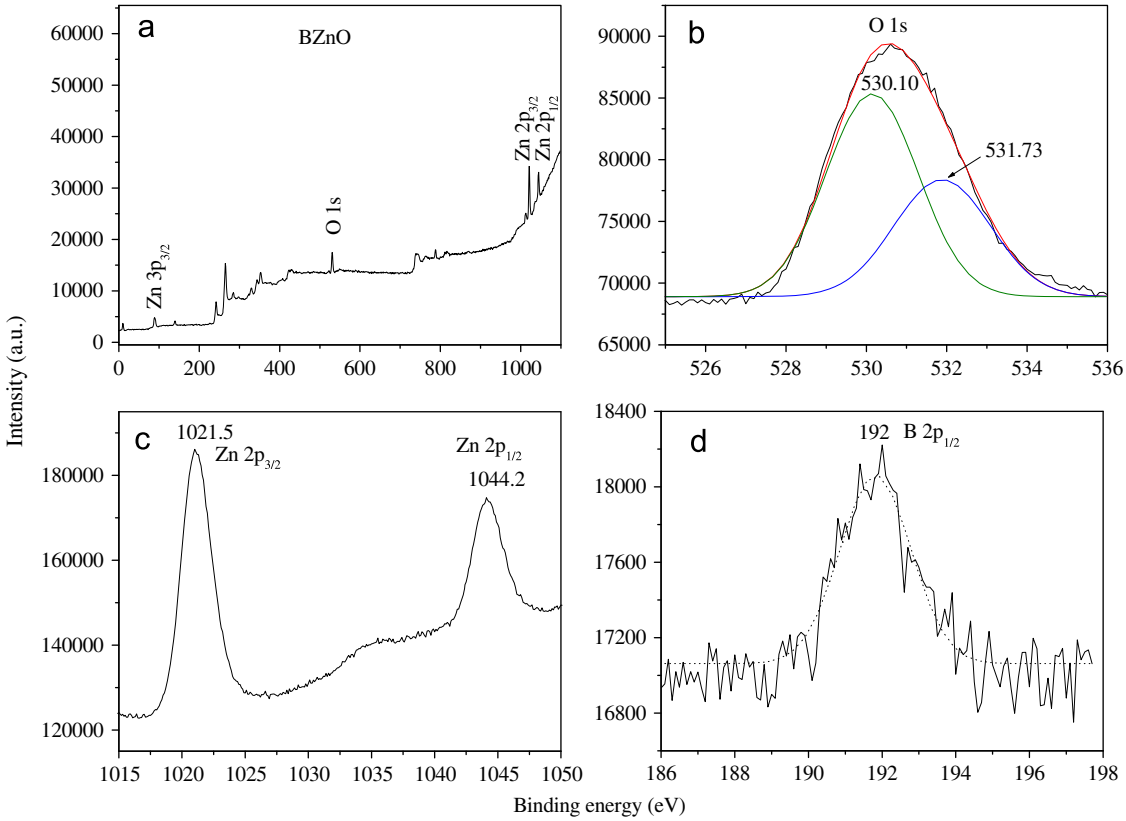


**Fig. 3.** XPS of B-doped ZnO: whole scanning XPS (a); High resolution O1s region (b); Zn 2p region (c); B 2p region (d) of B-doped ZnO.

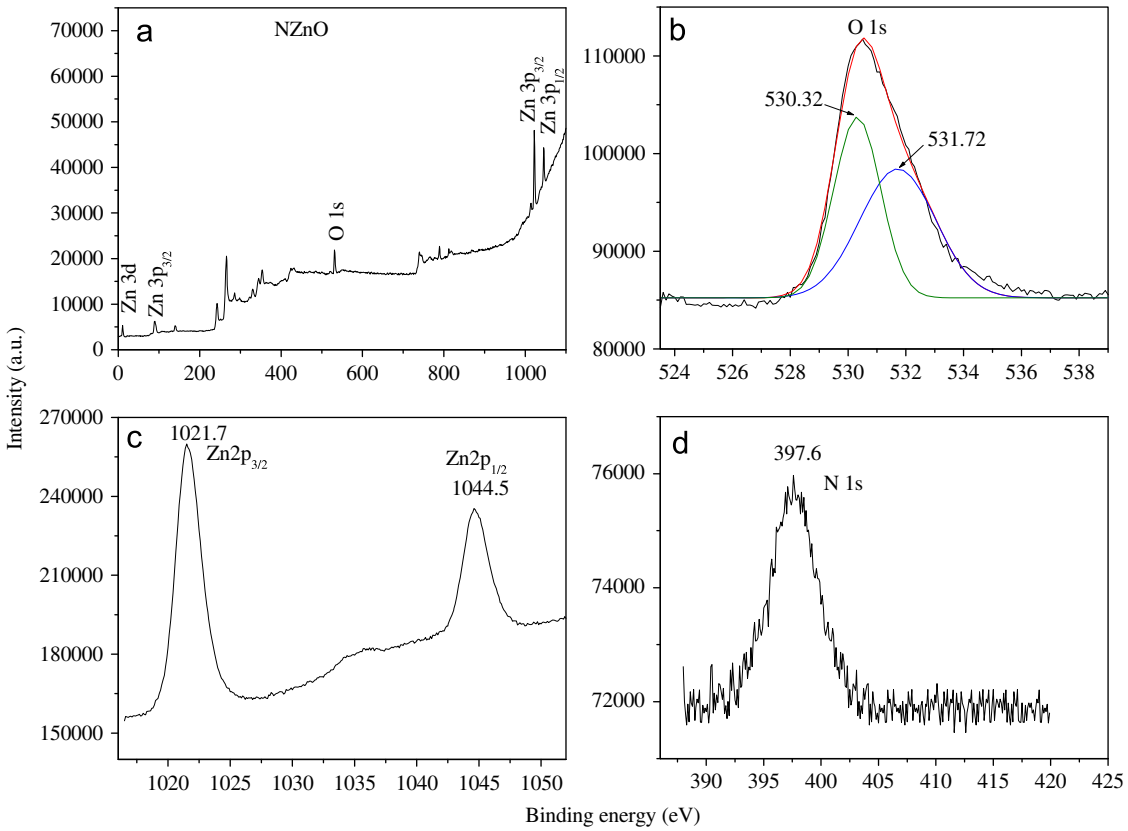


**Fig. 4.** XPS of N-doped ZnO: whole scanning XPS (a); High resolution O1s region (b); Zn 2p region (c); N1s region (d) of N-doped ZnO.

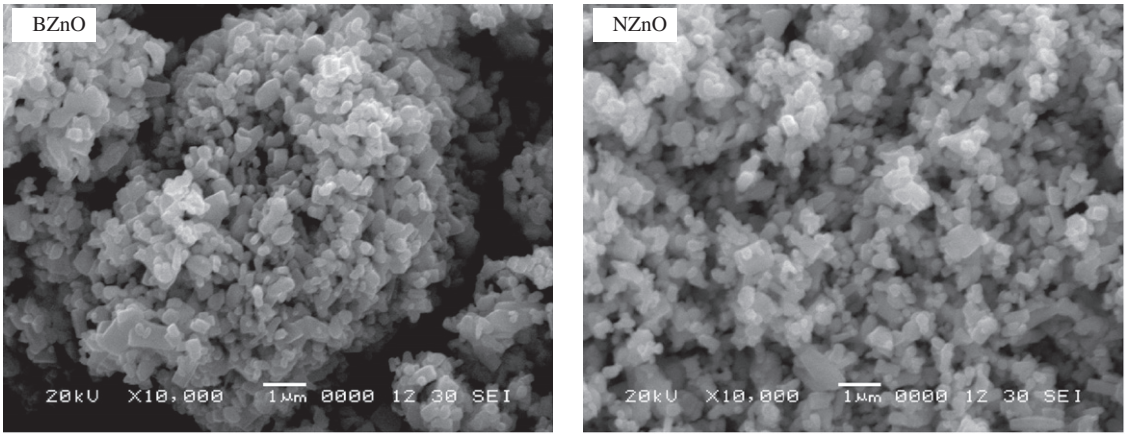


**Fig. 5.** SEM analysis of B-doped ZnO and N-doped ZnO.

are shown in Fig. 8. All the three samples exhibit UV emission band at about 390 nm, corresponding to the near band edge (NBE) emission, which is responsible for the recombination of the free excitons of ZnO. The excitonic peaks of B-doped and N-doped ZnO are broader than that of undoped ZnO. This broadening effect is because of lattice deformation in nonmetal doped ZnO as a result of substitution of some of the O sites by B or N. Similar results were reported by Shen et al. [19] during the PL measurements of semiconductor material. It is well known that the green yellow emission band between 450 and 480 nm originates from deep level (DL) defect emission associated with oxygen vacancies in ZnO lattices. Larger the content of oxygen vacancy or defect, stronger is the PL signal [20]. The intensity of green emission band is in the order of BZnO > NZnO > ZnO, which indicates that large number of oxygen vacancies or defects exists in B-doped ZnO.

### 3.3. Photocatalytic degradation study

Solar photocatalytic activity of pure and modified ZnO were evaluated by means of degradation of Bisphenol A (BPA), an endocrine disrupting chemical.

Blank experiments were carried out without photocatalyst to examine the extent of 100 ppm Bisphenol A (BPA100) undergoes 'photolysis' if photocatalyst was not used. There was no evidence of PCD of BPA100 in the absence of pure or modified ZnO. In the absence of light (in dark), when 100 ml of BPA100 containing 250 mg of pure or modified ZnO magnetically stirred for 300 min, 4% degradation was observed. For reference it is considered as zero time irradiation (Table 1). When aqueous solution of BPA100 containing photocatalyst was irradiated with sunlight, PCD was observed. The solar PCD of BPA100 was found to be maximum at

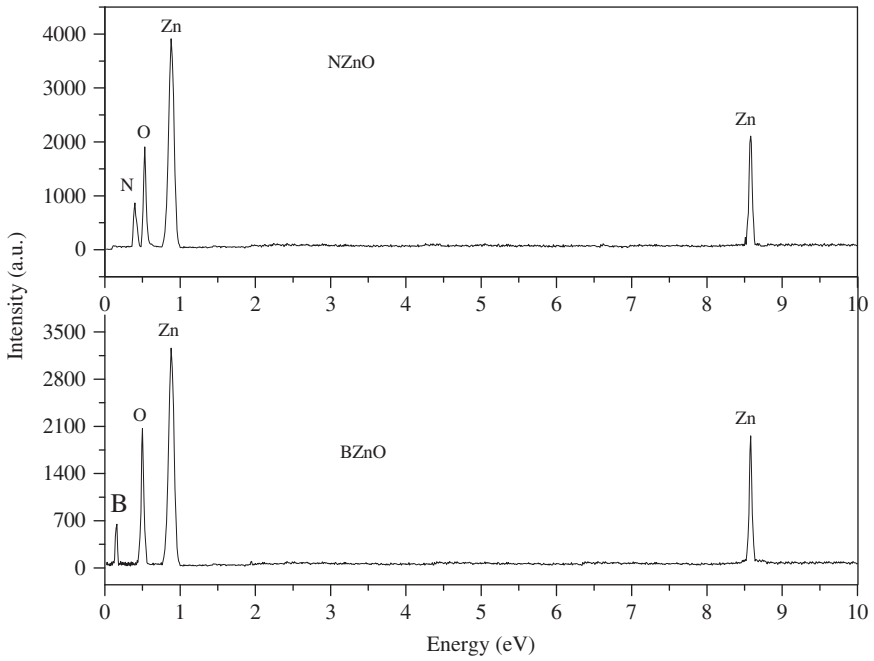


**Fig. 6.** EDX analysis of B-doped ZnO and N-doped ZnO.

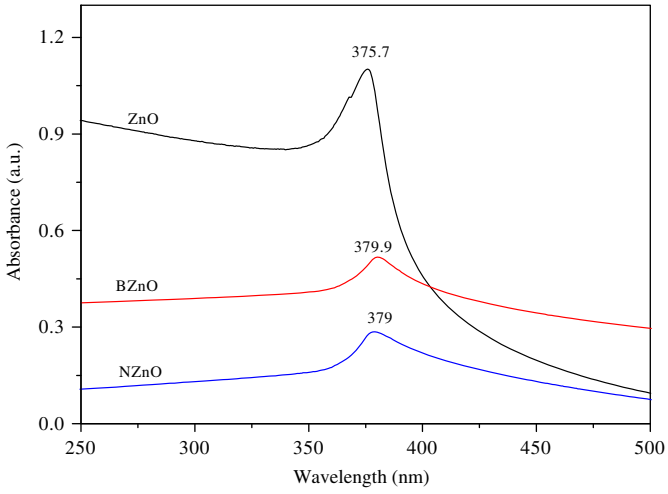


**Fig. 7.** UV–visible spectra of pure ZnO, B-doped ZnO and N-doped ZnO.

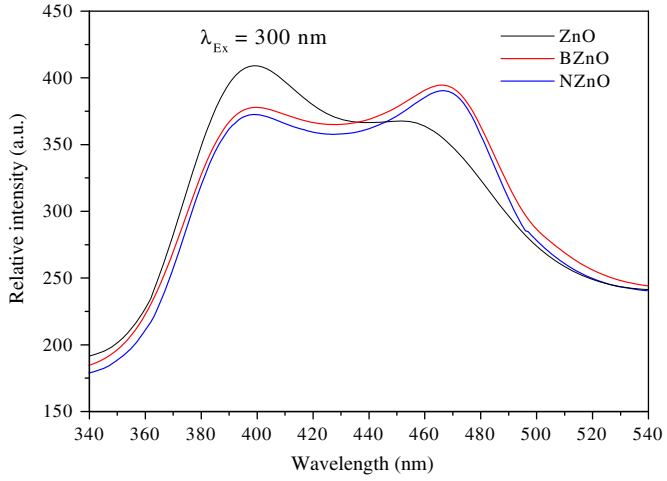


**Fig. 8.** Photoluminescence spectra of pure ZnO, B-doped ZnO and N-doped ZnO.

**Table 1**
Photocatalytic degradation efficiency of pure ZnO, NZnO and BZnO.

| Time | ZnO | | NZnO | | BZnO | |
|---|---|---|---|---|---|---|
| $t$ (min) | $COD_t$ (ppm) | $\eta$ (%) | $COD_t$ (ppm) | $\eta$ (%) | $COD_t$ (ppm) | $\eta$ (%) |
| 0 | 254 | 4 | 254 | 4 | 254 | 4 |
| 30 | 243 | 8 | 238 | 10 | 231 | 13 |
| 60 | 233 | 12 | 223 | 16 | 209 | 21 |
| 90 | 217 | 18 | 201 | 24 | 182 | 31 |
| 120 | 199 | 25 | 185 | 30 | 164 | 38 |
| 150 | 188 | 29 | 166 | 37 | 143 | 46 |
| 180 | 167 | 37 | 151 | 43 | 125 | 53 |
| 210 | 154 | 42 | 132 | 50 | 109 | 59 |
| 240 | 135 | 49 | 114 | 57 | 093 | 65 |
| 270 | 119 | 55 | 098 | 63 | 077 | 71 |
| 300 | 106 | 60 | 082 | 69 | 061 | 77 |

$COD_t$=Chemical oxygen demand at time $t$; $\eta$=photocatalytic degradation efficiency. [Bisphenol A]=100 ppm; initial COD of 100 ppm Bisphenol A ($COD_i$)=265 ppm; [Photocatalyst]=250 mg/100 ml; initial pH of the suspension=6.3 (without adjustment); intensity of sunlight=$1.7 \times 10^{-7}$ Einstein $s^{-1}$ $cm^{-2}$.

250 mg/100 ml of photocatalyst loading without adjustment of pH (natural pH of suspension=6.3). It was observed that with increase in sunlight irradiation time, PCD efficiency increases. The undoped, N-doped and B-doped ZnO showed 60%, 69% and 77% PCD efficiency, respectively, when reaction mixture was irradiated with sunlight for 300 min (Table 1). The doping of nonmetal into ZnO influences its photocatalytic activity, as the dopants can interfere with transport of photogenerated charge carriers. Hence the solar photocatalytic activity of nonmetal doped ZnO is greater than that of pure ZnO. Nonmetal doped ZnO contain higher oxygen vacancies or defects, less electron–hole recombination and narrow band gap than the undoped ZnO, which is seen in terms of absorption of light of longer wavelength. Unlike metal-ion dopants, non metal ion dopants such as N and B are less likely to form donor levels in the forbidden band but instead shift the valence band edge upward. This results in a narrowing of band gap. The additional electronic states that exist above the valence band edge of N- and B-doped ZnO are responsible for red shift absorption of these potential photocatalysts. In case of N-doped ZnO, the substitution of N for O, leads to the most effective

mixing of the 2*p* states of N with the 2*p* states of O which results in to the new valence band composed of O 2*p* orbitals at the lower-energy side and N 2*p* orbitals at the higher-energy side. Which ultimately leads to the band gap narrowing by shifting the valence band edge upward, this in return results in higher photocatalytic activity of N-doped ZnO in comparison with undoped ZnO in the visible-light region (sunlight). According to Braun et al. [21] an additional $e_g$ resonance in the valence band of semiconductor oxide is formed by nitrogen doping in the oxygen 1*s* pre-edge. This extra resonance was found to bear co responsibility for the photocatalytic performance of N-doped ZnO in sunlight. It is further to be noted that, the molecularly chemisorbed $N_2$ as well as substitutional N contributes to the visible light response of N-doped ZnO. However, the substitutional N was considered to be predominant factor in improving the photocatalytic activity under visible light [22]. Wang et al. [23] also pointed out that N in the form of Ti–N bond can extend the optical absorption of $TiO_2$ to visible region for N-doped $TiO_2$. The N-doped ZnO synthesized by mechanochemical method contain N in the form of Zn–N rather than Zn–O–N as discussed in Section 3.2.2 (XPS analysis) which also supports the better optical absorption and hence solar photocatalytic activity of N-doped ZnO. In case of B-doped ZnO, other than band gap narrowing, the doped boron could act as shallow traps for electrons, which prolong the lifetime of photo induced electrons and holes [24]. This leads to the enhancement of quantum efficiency of B-doped ZnO. Moreover, higher UV absorption and the greater number of oxygen vacancies in B-doped ZnO than that of N-doped ZnO in comparison to undoped ZnO as discussed in Section 3.2.4, are also supporting the better optical properties of BZnO. It is further to be noted that the shrinkage in crystallite planes and reduction in crystallite size of BZnO in comparison to NZnO and undoped ZnO (as discussed in Section 3.2.1) also contributes towards the enhancement of the solar PCD.

Fig. 9 shows a plot of $\ln(C_o/C)$ verses sunlight irradiation time ($t$) for PCD of BPA100 over pure and modified ZnO. The linearity of curves reveals that the PCD of BPA follows first order reaction kinetics. The apparent rate constants of PCD of BPA over BZnO is greater ($4.58\times10^{-3}\,h^{-1}$) than that over NZnO ($3.46\times10^{-3}\,h^{-1}$) and pure ZnO ($2.89\times10^{-3}\,h^{-1}$). Thus, the photocatalytic activity of BZnO determined in terms of the rate constant was also found to be higher than that of NZnO and pure ZnO.

### 3.4. Photocatalytic degradation mechanism

The excitation of photocatalyst by solar energy leads to the formation of an electron–hole pair (Scheme 1a). The hole combines with water to form ·OH radicals while electron converts the dissolved oxygen to super oxide radical ( $\cdot O_2^-$ ), a strong oxidizing species (Scheme 1b, c). The $\cdot O_2^-$ radicals are further converted into $HO_2\cdot$ and .OH species (Scheme 1d–f). The ·OH radicals thus formed during photo excitation shows electrophilic character and attack the electron rich C4 or C4′ positions in the phenyl groups of BPA (I), which results in the formation of 4-isopropyl phenol radical (II) and hydroquinone (III) ($m/z$=109+proton). Further oxidation of hydroquinone by ·OH radicals forms cyclohexa-1, 4-diene-1, 2, 4-triol radical (IV), which is converted in to benzene-1, 2, 4-triol (V) ($m/z$=125+proton) by reaction with dissolved oxygen. The 4-isopropyl phenol radical gets converted in to 4-(2-hydroxypropan-2-yl) phenol (VI) ($m/z$=151+proton) by reaction with ·OH radicals. The species (V) and (VI) are finally oxidized in to $CO_2$ and $H_2O$. The existence of (III), (V) and (VI) intermediates was also confirmed by HPLC analysis.

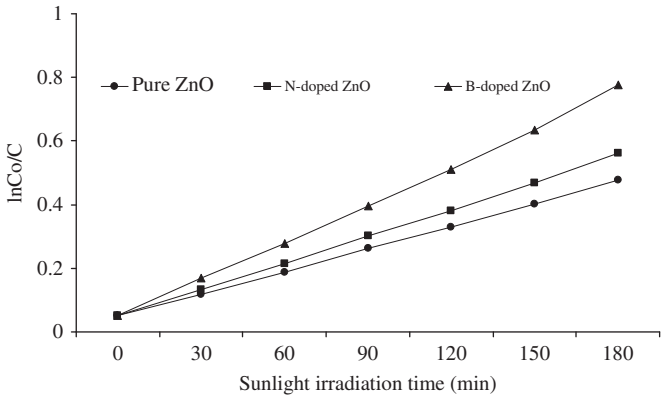


**Fig. 9.** Plot of $\ln(C_o/C)$ verses sunlight irradiation time ($t$) for PCD of Bisphenol A.

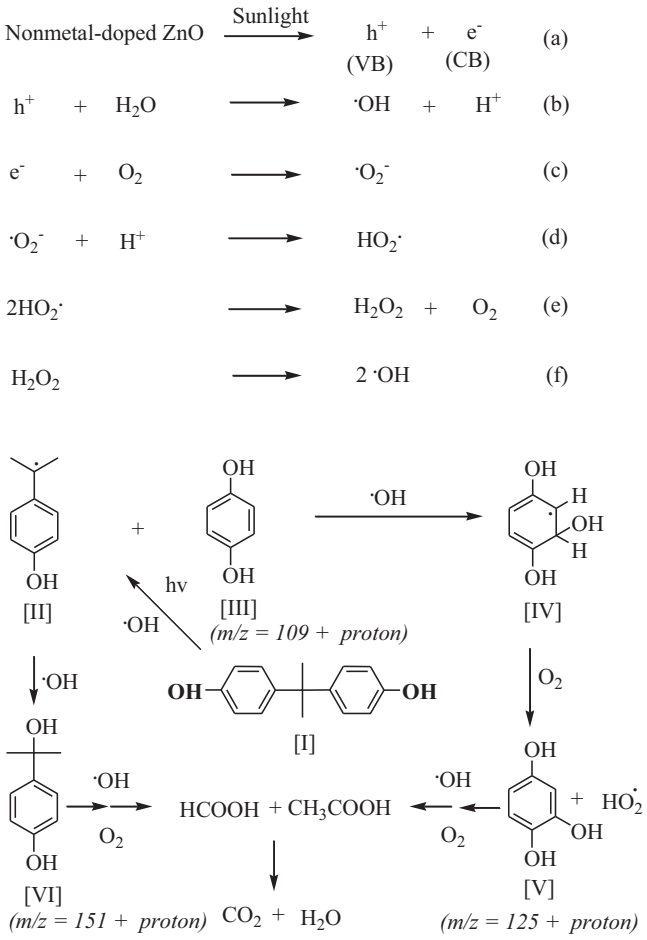


**Scheme 1.** Photocatalytic degradation mechanism of Bisphenol A .

## 4. Reuse of photocatalyst

The reuse of B-doped and N-doped ZnO was separately studied, by keeping all other parameters constant. During this study, after sunlight irradiation for 300 min, photoreaction mixture was centrifuged and filtered. Filtrate was used for COD determination and residue was washed several times with double distilled water in ultrasonic bath followed by filtration and drying at 110 °C in an electric oven. Recovered B-doped and N-doped ZnO was then reused for new PCD batch, without any further treatment such as heating in any kind of furnace. Activity of recycled B-doped and N-doped ZnO was found to retain even after fifth photo degradation experiment.

## 5. Conclusions

In present study BZnO and NZnO was synthesized by simple mechanochemical method. The incorporation of B or N in to ZnO was supported by broadening and lower Bragg angle shift in XRD pattern of these samples as compare to that of pure ZnO. The XPS of BZnO shows the peak positioned at 192 eV which was assigned for B $2p_{1/2}$ while, the peak at 397.6 eV was attributed to N 1*s* of NZnO. The band gap of pure ZnO (3.30 eV) becomes narrower for NZnO (3.27 eV) and BZnO (3.24 eV) as observed in UV–visible spectra. The room temperature PL spectra supports the number of defects and hence O vacancies in BZnO > NZnO > ZnO, which are correlated with photocatalytic activity. Photocatalytic degradation of BPA follows first order reaction kinetics and rate constants are in the order of: BZnO > NZnO > ZnO. Hydroquinone, benzene-1,2,4-triol and 4-(2-hydroxypropan-2-yl) phenol are identified as intermediates of PCD of Bisphenol A. Activity of recycled modified ZnO was found to retain even after fifth PCD experiment.

## Appendix A. Supporting materials

Supplementary data associated with this article can be found in the online version at doi:10.1016/j.jssc.2011.10.016.

## References

[1] E. Evgenidou, K. Fytianos, I. Poulios, Appl. Catal. B. Environ. 59 (2005) 81–89.
[2] S.K. Pardeshi, A.B. Patil, Sol. Energy 82 (2008) 700–705.
[3] D. Chatterjee, S. Dasgupta, J. Photochem. Photobiol. C: Photochem. Rev. 6 (2005) 186–205.
[4] B. Dindar, S. Icli, J. Photochem. Photobiol. A: Chem. 140 (2001) 263–268.
[5] S.K. Pardeshi, A.B. Patil, J. Mol. Catal. A: Chem. 308 (2009) 32–40.
[6] S.K. Pardeshi, A.B. Patil, J. Hazard. Mater. 163 (2009) 403–409.
[7] D.C. Reynolds, D.C. Look, B. Jogai, J.E. Hoelscher, J. Appl. Phys. 88 (2000) 2152.
[8] M.A. Behnajady, N. Modirshahla, R. Hamzavi, J. Hazard. Mater. B 133 (2006) 226–232.
[9] G.R. Li, T. Hu, G.L. Pan, T.Y. Yan, X.P. Gao, H.Y. Zhu, J. Phys. Chem. C 112 (31) (2008) 11859.
[10] J. Lu, Q. Zhang, J. Wang, F. Saito, M. Uchida, Powder Technol. 162 (2006) 33–37.
[11] B.N. Pawar, G. Cai, D. Ham, R.S. Mane, T. Ganesh, A. Ghule, R. Sharma, K.D. Jadhav, S.H. Han, Sol. Energy Mater. Sol. Cells 93 (2009) 524–527.
[12] L.C. Chen, Y.J. Tu, Y.S. Wang, R.S. Kan, C.M. Huang, J. Photochem. Photobiol. A: Chem. 199 (2008) 170–178.
[13] Q.W. Zhang, J. Wang, S. Yin, T. Sato, F. Saito, J. Am. Ceram. Soc. 87 (6) (2004) 1161–1163.
[14] A.B. Patil, K.R. Patil, S.K. Pardeshi, J. Hazard. Mater. 183 (2010) 315–323.
[15] J.T. Bellaire, G.A. Parr-Smith, Standard methods for the examination of water and wastewater, 7th ed., American Public Health Association, Washington D C, 1985.
[16] C.G. Hatchard, C.A. Parker, A new sensitive chemical actinometer II potassium ferrioxalate as a standard chemical actinometer, Proc. R. Soc. London A235 (518) (1956).
[17] C.H. Park, S.B. Zhang, S.H. Wei, Phys. Rev. B 66 (2002) 073202.
[18] X.H. Wang, S. Liu, P. Chang, Y. Tang, Phys. Lett. A 372 (2008) 2900–2903.
[19] W.Z. Shen, H.Z. Wu, P.J. McCann, J. Appl. Phys. 91 (2002) 3621–3625.
[20] J. Liqiang, Q. Yichun, W. Baiqi, L. Shudan, J. Baojiang, Y. Libin, F. Wei, F. Honggang, S. Jiazhong, Sol. Energy Mater. Sol. Cells 90 (2006) 1773–1787.
[21] A. Braun, K.K. Akurati, G. Fortunato, F.A. Reifler, A. Ritter, A.S. Harvey, A. Vital, T. Graule, J. Phys. Chem. C 114 (2010) 516.
[22] J. Yuan, M. Chen, J. Shi, W. Shangguan, J. Int., Hydrogen Energy 31 (2006) 1326.
[23] X. Wang, J.C. Yu, Y. Chen, L. Wu, X. Fu, Environ. Sci. Technol. 40 (2006) 2369–2374.
[24] X. Chen, S. Shen, L. Guo, S.S. Mao, Chem. Rev. 110 (2010) 6503–6570.